optica

Theory of chirped photonic crystals in biological broadband reflectors: supplementary material

CALEB Q. COOK[1,2] AND ARIEL AMIR[3]

[1] Department of Physics, Harvard University, Cambridge, Massachusetts 02138, USA
[2] Perimeter Institute for Theoretical Physics, Waterloo, Ontario N2J 2Y5, Canada
[3] School of Engineering and Applied Sciences, Harvard University, Cambridge, Massachusetts 02138, USA

Published 2 December 2016

This document provides supplementary information to "Theory of chirped photonic crystals in biological broadband reflectors," https://doi.org/10.1364/optica.3.001436. Included are details concerning the derivation of the WKB reflectance of ACPCs, the quantum scattering analogy for light reflectance of ACPCs, an additional, biologically relevant example of a reverse-engineered multilayer, and the image analysis procedure used to extract the bilayer optical thickness ratio from TEM images of ACPCs in nature.

https://doi.org/10.1364/optica.3.001436.s001

1. DERIVATION OF WKB REFLECTANCE

In this section, we outline the calculation of the WKB expression for the reflectance of adiabatic chirped photonic crystals presented in the main text. We also give the WKB reflectance calculated to the next order in ρ.

As presented in the main text, the wavelength-dependent bilayer transfer matrix $F_m(\lambda)$, relating the forward- and backward-propagating electric fields

$$\mathbf{E}_m = \begin{bmatrix} E_m^+ \\ E_m^- \end{bmatrix} \tag{S1}$$

via the vector recursion relation

$$\mathbf{E}_m = F_m(\lambda)\,\mathbf{E}_{m+1}, \tag{S2}$$

for our model takes the form

$$F_m(\lambda) = \begin{bmatrix} X_m(\lambda) & Y_m(\lambda) \\ Y_m^\star(\lambda) & X_m^\star(\lambda) \end{bmatrix} \tag{S3}$$

with complex matrix elements $X_m(\lambda)$, $Y_m(\lambda)$ satisfying $\det F_m(\lambda) = |X_m|^2 - |Y_m|^2 = 1$. The eigenvectors $\mathbf{w}_m^\pm$ and corresponding eigenvalues $\mu_m^\pm$ of the general transfer matrix F_m are explicitly

$$\mathbf{w}_m^\pm = D_m^\pm \begin{bmatrix} 1 \\ \left(\dfrac{\mu_m^\pm - X_m}{Y_m}\right) \end{bmatrix} \tag{S4}$$

$$\mu_m^\pm = \left(\frac{X_m + X_m^\star}{2}\right) \pm \sqrt{\left(\frac{X_m + X_m^\star}{2}\right)^2 - 1}, \tag{S5}$$

where the $D_m^\pm$ are arbitrary eigenvector normalizations.

In the main text it is shown that linear combinations of modulated Bloch waves

$$\mathbf{E}_m = \sum_{i=\pm} C^i \exp\left[-\int^m \ln \mu_k^i \mathrm{d}k\right] \mathbf{w}_m^i \tag{S6}$$

approximately solve the transfer matrix recursion (S2) in the limit of adiabatic chirp. One could proceed by seeking higher-order corrections to the modulated Bloch wave solution (S6), but we instead invoke energy conservation to find the m-dependence of the eigenvector normalizations $D_m^\pm$ and thereby extract the dominant effect of these corrections [1]. From Eqs. (S5) and (S6) we calculate the Poynting energy flux density $\mathcal{P}_m \propto |E_m^+|^2 - |E_m^-|^2$ [2] to be

$$\mathcal{P}_m \propto \begin{cases} |\mathcal{C}^+|^2 \, |D_m^+|^2 \left(\dfrac{\mu_m^+ - \mu_m^-}{\mu_m^+ - X_m^\star} \right) - |\mathcal{C}^-|^2 \, |D_m^-|^2 \left(\dfrac{\mu_m^+ - \mu_m^-}{\mu_m^- - X_m^\star} \right) & \text{(passband)} \\ \left(\mathcal{C}^+ D_m^+\right) \left(B D_m^-\right)^\star \left(\dfrac{\mu_m^+ - \mu_m^-}{\mu_m^+ - X_m^\star} \right) - \left(\mathcal{C}^+ D_m^+\right)^\star \left(\mathcal{C}^- D_m^-\right) \left(\dfrac{\mu_m^+ - \mu_m^-}{\mu_m^- - X_m^\star} \right) & \text{(stopband)} \end{cases} \tag{S7}$$

which *a priori* defpends on the bilayer index m. However, taking the eigenvector normalizations $D_m^\pm$ to scale as

$$D_m^\pm \sim \sqrt{\frac{\mu_m^\pm - X_m^\star}{\mu_m^+ - \mu_m^-}}. \tag{S8}$$

removes the m-dependence of $\mathcal{P}_m = \mathcal{P}$ (S7) and therefore enforces constant energy flux density in the multilayer, as required by energy conservation. The modulated Bloch wave solution (S6) with the eigenvector normalizations (S8) is a generalization of the Bremmer method for deriving WKB-type solutions [3, 4].

As a turning point $m \to m_{1,2}$ in the multilayer is approached, the transfer matrix eigenvalues (S5) $\mu_m^+ \to \mu_m^-$ converge to one another and the required eigenvector normalizations $D_m^\pm$ (S8) become arbitrarily large. This implies that our assumption of slowly varying transfer matrix eigenvectors $\mathbf{w}_m^\pm$ breaks down and our approximate solution (S6) no longer holds near the turning points $m \sim m_{1,2}$, even in the case of adiabatic chirp. We must therefore write general solutions of the form (S6) separately in the three regions of the multilayer separated by the turning points m_1 and m_2, giving

$$\begin{bmatrix} E_m^+ \\ E_m^- \end{bmatrix} = \begin{cases} A \exp\left\{ i \int_m^{m_1} \cos^{-1}\left(\frac{a_k}{2}\right) \mathrm{d}k \right\} \mathbf{w}_m^+ + B \exp\left\{ -i \int_m^{m_1} \cos^{-1}\left(\frac{a_k}{2}\right) \mathrm{d}k \right\} \mathbf{w}_m^- & (m < m_1) \\ (-1)^m \left[C \exp\left\{ \int_{m_1}^m \cosh^{-1}\left(-\frac{a_k}{2}\right) \mathrm{d}k \right\} \mathbf{w}_m^- + D \exp\left\{ -\int_{m_1}^m \cosh^{-1}\left(-\frac{a_k}{2}\right) \mathrm{d}k \right\} \mathbf{w}_m^+ \right] & (m_1 < m < m_2) \\ F \exp\left\{ -i \int_{m_2}^m \cos^{-1}\left(\frac{a_k}{2}\right) \mathrm{d}k \right\} \mathbf{w}_m^+ + G \exp\left\{ i \int_{m_2}^m \cos^{-1}\left(\frac{a_k}{2}\right) \mathrm{d}k \right\} \mathbf{w}_m^- & (m_2 < m) \end{cases} \tag{S9}$$

where we have introduced the complex coefficients A, B, C, D, F, and G, in addition to the trace $a_m(\lambda) \equiv \mathrm{Tr}\,[F_m(\lambda)]$ whose magnitude determines the complex structure of the transfer matrix eigenvalues $\mu_m^\pm$, so that

$$\begin{cases} |a_m(\lambda)| < 2 \iff m \in \text{passband} \\ |a_m(\lambda)| > 2 \iff m \in \text{stopband} \\ |a_m(\lambda)| = 2 \iff m \text{ is a turning point} \end{cases} \tag{S10}$$

Since our modulated Bloch wave solution (S9) breaks down near turning points $m \sim m_{1,2}$, we return to the exact vector recurrence (S2), which may be approximated in the limit of adiabatic chirp as

$$\mathbf{E}_{m+1} + \mathbf{E}_{m-1} = \left(F_m^{-1} + F_{m-1} \right) \mathbf{E}_m \approx a_m \mathbf{E}_m \tag{S11}$$

in the vicinity of a given bilayer m. This implies that we can treat $E_m^\pm$ as decoupled fields each independently satisfying the recurrence relation

$$E_{m+1}^\pm = a_m E_m^\pm - E_{m-1}^\pm \tag{S12}$$

near turning points $m \sim m_{1,2}$. A discrete form of the Wentzel-Kramers-Brillouin (WKB) method [5–9] then allows us to approximately solve Eq. (S12) in the vicinity of turning points $m \sim m_{1,2}$ and match the modulated Bloch waves (S9) across the stopband region $m \in [m_1, m_2]$.

The discrete WKB method has traditionally found application in approximate calculations of quantum mechanical energy spectra [1, 6, 9, 10]. The discrete WKB method in the present context is detailed in Section 3, with discrete WKB solutions to the difference equation (S12) given by Eq. (S36).

Crucially, the discrete WKB solutions (S36) share the same functional form as the modulated Bloch waves (S9) in the vicinity of a turning point $m \sim m_{1,2}$, since in that limit the transfer matrix eigenvector normalizations (S8) become

$$D_m^+ \sim D_m^- \sim (\mu_m^+ - \mu_m^-)^{-1/2} = (a_m^2 - 4)^{-1/4} \tag{S13}$$

and Eq. (S9) subsequently reduces to the discrete WKB solutions (S36). We therefore identify the complex coefficients $A, \ldots, G$ in the modulated Bloch wave solution (S9) with the analogous coefficients in the discrete WKB solution (S36). Applying an asymptotic matching procedure to the discrete WKB solution coefficients, and hence the modulated Bloch wave coefficients A, B, F, and G, then allows for patching of the modulated Bloch waves (S9) across the stopband region.

Asymptotic matching of the discrete WKB solutions is performed in Section 3, and the resulting connection formulae across an $x_m \approx 1$ (or more generally, $a_m < -2$) stopband $m \in [m_1, m_2]$ are given by

$$\begin{bmatrix} A \\ B \end{bmatrix} = \begin{bmatrix} \alpha & \beta \\ \beta^\star & \alpha^\star \end{bmatrix} \begin{bmatrix} F \\ G \end{bmatrix} \tag{S14}$$

where we have introduced the variables

$$\alpha(\lambda) = e^{i[m_2(\lambda) - m_1(\lambda)]\pi} \left[e^{\gamma(\lambda)} + \frac{1}{4} e^{-\gamma(\lambda)} \right] \tag{S15}$$

$$\beta(\lambda) = -i e^{-i[m_2(\lambda) + m_1(\lambda)]\pi} \left[e^{\gamma(\lambda)} - \frac{1}{4} e^{-\gamma(\lambda)} \right] \tag{S16}$$

$$\gamma(\lambda) = \int_{m_1(\lambda)}^{m_2(\lambda)} \cosh^{-1}\left[-\frac{a_m(\lambda)}{2} \right] \mathrm{d}m \tag{S17}$$

The parameter γ is analogous to the tunneling exponent in the Gamow theory of alpha decay [11], in which the probability T of He^{2+} emission from an atomic nucleus satisfies $T \sim e^{-2\gamma}$.

In the present case, $\gamma(\lambda)$ (S17) characterizes how deeply light of wavelength λ penetrates an $a_m < -2$ stopband of a chirped photonic crystal.

The terminating absorber condition $E_N^- = 0$ assumed in our model gives a linear relation between the coefficients F and G in the modulated Bloch wave solution (S9) and thus a linear relation between the coefficients A and B via the discrete WKB matching formulae (S14). This linear relation fixes A/B and hence the field ratio $r = E_0^-/E_0^+$ through the modulated Bloch wave solution (S9). The reflectance $R = |r|^2$ of ACPCs calculated in this way is given by

$$R(\lambda) = \widetilde{R}(\lambda) + 2\rho\sqrt{\widetilde{R}(\lambda)}\left[1-\widetilde{R}(\lambda)\right]\left\{\frac{\sin(2\pi\ell_0/\lambda)}{\sin[2\pi(1+\Xi)\ell_0/\lambda]}\sin 2\phi_0 - \frac{\sin(2\pi\ell_N/\lambda)}{\sin[2\pi(1+\Xi)\ell_N/\lambda]}\sin 2\phi_N\right\} + \mathcal{O}\left(\rho^2\right) \quad \textbf{(S18)}$$

where we have again introduced the zeroth-order WKB reflectance

$$\widetilde{R}(\lambda) = 1 - \exp[-2\gamma(\lambda)]. \quad \textbf{(S19)}$$

as well as the phase angles

$$\phi_0(\lambda) = \int_0^{m_1(\lambda)} \cos^{-1}\left[\frac{a_m(\lambda)}{2}\right] \mathrm{d}m - m_1(\lambda)\pi \quad \textbf{(S20)}$$

$$\phi_N(\lambda) = \int_{m_2(\lambda)}^{N} \cos^{-1}\left[\frac{a_m(\lambda)}{2}\right] \mathrm{d}m + m_2(\lambda)\pi \quad \textbf{(S21)}$$

2. TIGHT-BINDING ANALOGY

In this section, we make an analogy between the electric fields $E_m^{\pm}$ in an adiabatically chirped photonic crystal and the zero energy eigenmodes of a one-dimensional chain, described quantum mechanically by a tight-binding Hamiltonian. Naively applying the continuous WKB method to the quantum chain yields results consistent with those of the discrete WKB analysis near turning points and offers insight into the functional form of $E_m^{\pm}$ and our matching formulae. By taking a continuum limit of the quantum chain tight-binding Hamiltonian, we also make concrete the analogy between the reflection of light from a photonic stopband and quantum scattering from a potential barrier.

We note that the recurrence relation (S12) is precisely the equation one would obtain by seeking the zero energy eigenmodes E_m of a Hamiltonian H given by

$$H = \begin{bmatrix} a_1 & -1 & & & \\ -1 & a_2 & \ddots & & \\ & -1 & \ddots & -1 & \\ & & \ddots & a_{N-1} & -1 \\ & & & -1 & a_N \end{bmatrix}. \quad \textbf{(S22)}$$

We can view the matrix H as a tight-binding Hamiltonian of a finite, one-dimensional quantum chain with nearest-neighbor hopping elements [12].

Let us first begin with the simple case that $a_m = a$ is constant. In this case, we can write the exact eigenmode solution as a discrete plane wave $E_m = e^{\pm i\kappa m}$ with wavevector κ. Substitution into our recurrence relation (S12) then tells us that

$$e^{i\kappa} + e^{-i\kappa} = a \quad \textbf{(S23)}$$

which implies that our wavevector κ is given by

$$\kappa = \begin{cases} \cos^{-1}(a/2), & a \in [-2,2] \\ i\cosh^{-1}(a/2), & a > 2 \\ i\cosh^{-1}(a/2) + \pi, & a < -2 \end{cases}. \quad \textbf{(S24)}$$

The general eigenmode solution E_m in the constant $a_m = a$ case is then just a linear superposition

$$E_m = Ae^{i\kappa m} + Be^{-i\kappa m} \quad \textbf{(S25)}$$

of the discrete plane waves of wavevectors $\pm\kappa$. When $a \in [-2,2]$ and κ is real, the zero energy eigenmode components E_m are oscillatory in the bilayer/chain site index m. Conversely, when $|a| > 2$ and κ is imaginary, the components E_m are the sum of growing and decaying exponentials in the index m.

In the more general case that a_m varies slowly with bilayer/chain site index m, we can write the continuous WKB solution to the above eigenmode problem as [11]

$$E_m \propto \frac{1}{\sqrt{\kappa_m}} e^{\pm i\int^m \kappa_k \mathrm{d}k}. \quad \textbf{(S26)}$$

Substituting this expression into our recursion relation gives, to lowest order in the variation of κ_m with respect to m, the same consistency equation as before

$$e^{i\kappa_m} + e^{-i\kappa_m} = a_m \quad \textbf{(S27)}$$

which implies (variable) wavevector solutions

$$\kappa_m = \begin{cases} \cos^{-1}(a_m/2), & a_m \in [-2,2] \\ i\cosh^{-1}(a_m/2), & a_m > 2 \\ i\cosh^{-1}(a_m/2) + \pi, & a_m < -2 \end{cases}. \quad \textbf{(S28)}$$

Again, the magnitude of a_m tells us whether the the eigenmode components E_m are oscillatory or exponential in the index m.

Comparing the continuum WKB result (S26) with the form of E_m obtained via the discrete WKB method (S36), we see that the two differ only by the m-dependence of the passband magnitude $|E_m|$ of the electric field/zero energy eigenmode. In particular,

$$|E_m| = \begin{cases} \left[\cos^{-1}(a_m/2)\right]^{-1/2} & \text{(S26)} \\ \left(4-a_m^2\right)^{-1/4} & \text{(S36)} \end{cases} \quad \textbf{(S29)}$$

in passband regions $|a_m| < 2$. However, these two forms are consistent to lowest order in $(a_m \pm 2)$, i.e. near turning points, which is precisely the regime in which the difference equation (S12) is applied in Section 3 to match the modulated Bloch waves (S9). This explains the strong similarity (exact agreement) between

the standard WKB connection formulae [11] and the discrete WKB matching formulae across an odd (even) stopband and given in Section 3.

We can gain further intuition from this tight-binding analogy by rewriting the tight-binding Hamiltonian H in the continuum limit as

$$H \to -\frac{\mathrm{d}^2}{\mathrm{d}z^2} + [a(z) - 2] = \left(-i\frac{\mathrm{d}}{\mathrm{d}z}\right)^2 + V(z) \tag{S30}$$

where $m \to z$ represents the continuous coordinate parametrizing the depth in the multilayer and/or length along the quantum chain, and we have introduced the potential

$$V(z) = a(z) - 2. \tag{S31}$$

Examining the continuum quantum chain potential $V(z)$ reveals why one obtains evanescent solutions when $a(z) > 2$; in this case the potential (S31) is positive, and therefore the zero energy modes we seek are classically forbidden by energy conservation. In quantum mechanics, however, such classically forbidden solutions to $HE(z) = 0$ are allowed, but are exponentially damped in z due to quantum tunneling [11].

An identical analogy can be made for odd $a(z) < -2$ stopbands by transforming the recurrence (S12) in E_m to the recurrence

$$-\widetilde{E}_{m+1} + \widetilde{a}_m \widetilde{E}_m - \widetilde{E}_{m-1} = 0 \tag{S32}$$

in the transformed variable $\widetilde{E}_m = (-1)^m E_m$, where have defined $\widetilde{a}(z) = -a(z)$. Repeating the same analysis as before, we arrive at the odd stopband potential

$$\widetilde{V}(z) = \widetilde{a}(z) - 2 = -a(z) - 2 \tag{S33}$$

which is plotted in the main text.

We therefore conclude that stopbands in adiabatically chirped photonic crystals are analogous to the classically forbidden regions on a one-dimensional tight-binding quantum chain, with light scattering from the former corresponding to quantum tunneling through the latter.

3. DERIVATION OF DISCRETE WKB CONNECTION FORMULAE

In this section, we first derive the discrete WKB connection formulae across an even, i.e. $a_m > 2$, stopband and then apply a transformation to the recurrence (S12) to obtain the analogous connection formulae across an odd, $a_m < -2$, stopband. These results connect *scattering* states $E_m^{\pm}$ across a classically forbidden region and augment the discrete WKB matching procedure used by Braun [6] to derive the quantization rules for *bound* states.

Since both E_m^+ and E_m^- (approximately) satisfy the same recursion relation

$$E_{m+1}^{\pm} = a_m E_m^{\pm} - E_{m-1}^{\pm} \tag{S34}$$

near a turning point $m \sim m_{1,2}$, it suffices to consider just E_m^+. Approximate discrete WKB expressions for the field E_m^+ can be obtained by assuming a solution to the above recurrence relation of the form

$$E_m^+ = \exp\left\{i\left[\Phi_m^0 + \Phi_m^1 + \Phi_m^2 + \cdots\right]\right\} \tag{S35}$$

where the unknown functions Φ_m^j are labeled according to their rate of change with respect to the index m, so that $\dot{\Phi}_m^j = \mathcal{O}\left(m^{-j}\right)$, $\ddot{\Phi}_m^j = \mathcal{O}\left(m^{-j-1}\right)$, and so on. Substituting the discrete WKB ansatz (S35) into the recurrence relation (S34) and solving for the unknown functions Φ_m^j up to order $\mathcal{O}\left(m^{-1}\right)$ yields [6, 9]:

$$E_m^+ = \begin{cases} \dfrac{1}{\sqrt[4]{4 - a_m^2}}\left[A\exp\left\{i\int_m^{m_1}\cos^{-1}\left(\dfrac{a_k}{2}\right)\mathrm{d}k\right\} + B\exp\left\{-i\int_m^{m_1}\cos^{-1}\left(\dfrac{a_k}{2}\right)\mathrm{d}k\right\}\right] & (m < m_1) \\ \dfrac{1}{\sqrt[4]{a_m^2 - 4}}\left[C\exp\left\{\int_{m_1}^{m}\cosh^{-1}\left(\dfrac{a_k}{2}\right)\mathrm{d}k\right\} + D\exp\left\{-\int_{m_1}^{m}\cosh^{-1}\left(\dfrac{a_k}{2}\right)\mathrm{d}k\right\}\right] & (m_1 < m < m_2) \\ \dfrac{1}{\sqrt[4]{4 - a_m^2}}\left[F\exp\left\{-i\int_{m_2}^{m}\cos^{-1}\left(\dfrac{a_k}{2}\right)\mathrm{d}k\right\} + G\exp\left\{i\int_{m_2}^{m}\cos^{-1}\left(\dfrac{a_k}{2}\right)\mathrm{d}k\right\}\right] & (m_2 < m) \end{cases} \tag{S36}$$

Our goal is to match these solutions across the stopband, i.e. find a linear relationship between the coefficients A, B and F, G. Performing this matching procedure will require analysis of approximate solutions to original recurrence (S12) in the vicinity of each turning turning point, which we obtain by linearizing a_m near m_1 and m_2.

A. Even Stopband Connection Formulae

Suppose we have an $a_m > 2$ stopband for $m \in [m_1, m_2]$ (where m_1, m_2 are not necessarily integers), surrounded on either side by propagation bands $|a_m| < 2$.

A.1. Matching Across Even $m = m_1$ Turning Point

When linearized near m_1, the recurrence (S12) takes the form

$$E_{m+1}^+ = [2 + \alpha_1(m - m_1)]E_m^+ - E_{m-1}^+ \quad (\text{for } m \text{ near } m_1) \tag{S37}$$

for some $\alpha_1 > 0$ determined by a_m, or equivalently

$$E^+_{m+1} = \frac{2\nu}{x} E^+_m - E^+_{m-1} \quad (\text{for } m \text{ near } m_1) \tag{S38}$$

where we have defined $\nu \equiv x + (m - m_1)$ and $x \equiv 2/\alpha_1$. In terms of the variables ν and x, the solution to this recurrence is a linear combination of the Bessel functions $E^+_m = aJ_\nu(x) + bY_\nu(x)$. Now, the asymptotic expansions of the Bessel functions $J_\nu(x)$ and $Y_\nu(x)$ for large argument x (consistent with small α_1 and hence slow chirp) and large order ν (consistent with m far from m_1) depend on the relative magnitude of x and ν. In each case, the asymptotic expansions are given by (see [13], 9.3.2 and 9.3.3):

$$J_\nu(x) \approx \begin{cases} \sqrt{\frac{2}{\pi}} \left(x^2 - \nu^2\right)^{-1/4} \cos\left[-\nu \cos^{-1}\left(\frac{\nu}{x}\right) + \sqrt{x^2 - \nu^2} - \frac{\pi}{4}\right] & (\nu < x) \\ \sqrt{\frac{1}{2\pi}} \left(\nu^2 - x^2\right)^{-1/4} \exp\left[-\nu \cosh^{-1}\left(\frac{\nu}{x}\right) + \sqrt{\nu^2 - x^2}\right] & (\nu > x) \end{cases} \tag{S39}$$

$$Y_\nu(x) \approx \begin{cases} \sqrt{\frac{2}{\pi}} \left(x^2 - \nu^2\right)^{-1/4} \sin\left[-\nu \cos^{-1}\left(\frac{\nu}{x}\right) + \sqrt{x^2 - \nu^2} - \frac{\pi}{4}\right] & (\nu < x) \\ -\sqrt{\frac{2}{\pi}} \left(\nu^2 - x^2\right)^{-1/4} \exp\left[\nu \cosh^{-1}\left(\frac{\nu}{x}\right) - \sqrt{\nu^2 - x^2}\right] & (\nu > x) \end{cases} \tag{S40}$$

We can then express these Bessel function expansions in terms of the original variables m, m_1, and α by noting $\left(\nu^2 - x^2\right) = \left(a_m^2 - 4\right)/\alpha_1^2$ in the linearized region and applying the change of variable $k \to k + m_1 - x$ to obtain

$$\nu \cos^{-1}\left(\frac{\nu}{x}\right) - \sqrt{x^2 - \nu^2} = \int_\nu^x \cos^{-1}\left(\frac{k}{x}\right) \mathrm{d}k = \int_m^{m_1} \cos^{-1}\left(\frac{a_k}{2}\right) \mathrm{d}k \tag{S41}$$

$$\nu \cosh^{-1}\left(\frac{\nu}{x}\right) - \sqrt{\nu^2 - x^2} = \int_x^\nu \cosh^{-1}\left(\frac{k}{x}\right) \mathrm{d}k = \int_{m_1}^m \cosh^{-1}\left(\frac{a_k}{2}\right) \mathrm{d}k \tag{S42}$$

Combining these results, the Bessel function asymptotic expansions can be rewritten as

$$J_\nu(x) \approx \begin{cases} \sqrt{\frac{2\alpha_1}{\pi}} \left(4 - a_m^2\right)^{-1/4} \cos\left[-\int_m^{m_1} \cos^{-1}\left(\frac{a_k}{2}\right) \mathrm{d}k - \frac{\pi}{4}\right] & (m < m_1) \\ \sqrt{\frac{\alpha_1}{2\pi}} \left(a_m^2 - 4\right)^{-1/4} \exp\left[-\int_{m_1}^m \cosh^{-1}\left(\frac{a_k}{2}\right) \mathrm{d}k\right] & (m > m_1) \end{cases} \tag{S43}$$

$$Y_\nu(x) \approx \begin{cases} \sqrt{\frac{2\alpha_1}{\pi}} \left(4 - a_m^2\right)^{-1/4} \sin\left[-\int_m^{m_1} \cos^{-1}\left(\frac{a_k}{2}\right) \mathrm{d}k - \frac{\pi}{4}\right] & (m < m_1) \\ -\sqrt{\frac{2\alpha_1}{\pi}} \left(a_m^2 - 4\right)^{-1/4} \exp\left[\int_{m_1}^m \cosh^{-1}\left(\frac{a_k}{2}\right) \mathrm{d}k\right] & (m > m_1) \end{cases} \tag{S44}$$

so that the linear combination of Bessel functions $E^+_m = aJ_\nu(x) + bY_\nu(x)$ therefore becomes

$$E^+_m = \begin{cases} \frac{1}{\sqrt[4]{4 - a_m^2}} \left[\sqrt{\frac{\alpha_1}{2\pi}} \left(a e^{i\pi/4} - b e^{-i\pi/4}\right) \exp\left\{i \int_m^{m_1} \cos^{-1}\left(\frac{a_k}{2}\right) \mathrm{d}k\right\} + \text{C.C.}\right] & (m < m_1) \\ \frac{1}{\sqrt[4]{a_m^2 - 4}} \left[-b\sqrt{\frac{2\alpha_1}{\pi}} \exp\left\{\int_{m_1}^m \cosh^{-1}\left(\frac{a_k}{2}\right) \mathrm{d}k\right\} + a\sqrt{\frac{\alpha_1}{2\pi}} \exp\left\{-\int_{m_1}^m \cosh^{-1}\left(\frac{a_k}{2}\right) \mathrm{d}k\right\}\right] & (m > m_1) \end{cases} \tag{S45}$$

as our asymptotic solution for the field E^+_m near the turning point m_1. Comparing this result with the relevant regions of our discrete WKB solution (S36) and eliminating the intermediate coefficients a and b yields

$$A = e^{-i\pi/4} \left(\frac{C}{2} + iD\right) \tag{S46}$$

$$B = e^{+i\pi/4} \left(\frac{C}{2} - iD\right)$$

These are the matching relations across the $m = m_1$ turning point.

A.2. Matching Across Even $m = m_2$ Turning Point

We define the even stopband tunneling parameter

$$\gamma = \int_{m_1}^{m_2} \cosh^{-1}\left(\frac{a_m}{2}\right) \mathrm{d}m. \tag{S47}$$

Using γ, we can then rewrite the discrete WKB solution (S36) as

$$E^+_m = \begin{cases} \frac{1}{\sqrt[4]{4 - a_m^2}} \left[A \exp\left\{i \int_m^{m_1} \cos^{-1}\left(\frac{a_k}{2}\right) \mathrm{d}k\right\} + B \exp\left\{-i \int_m^{m_1} \cos^{-1}\left(\frac{a_k}{2}\right) \mathrm{d}k\right\}\right] & (m < m_1) \\ \frac{1}{\sqrt[4]{a_m^2 - 4}} \left[De^{-\gamma} \exp\left\{\int_m^{m_2} \cosh^{-1}\left(\frac{a_k}{2}\right) \mathrm{d}k\right\} + Ce^{\gamma} \exp\left\{-\int_m^{m_2} \cosh^{-1}\left(\frac{a_k}{2}\right) \mathrm{d}k\right\}\right] & (m_1 < m < m_2) \\ \frac{1}{\sqrt[4]{4 - a_m^2}} \left[F \exp\left\{-i \int_{m_2}^m \cos^{-1}\left(\frac{a_k}{2}\right) \mathrm{d}k\right\} + G \exp\left\{i \int_{m_2}^m \cos^{-1}\left(\frac{a_k}{2}\right) \mathrm{d}k\right\}\right] & (m_2 < m) \end{cases} \tag{S48}$$

This reformulation is useful for matching near $m = m_2$, since the discrete WKB solution in the stopband is now expressed as a function of right turning point m_2. The recurrence (S12) linearized near $m = m_2$ takes the form

$$E^+_{m+1} = [2 - \alpha_2 (m - m_2)] E^+_m - E^+_{m-1} \quad (\text{for } m \text{ near } m_2) \tag{S49}$$

or equivalently,

$$\widetilde{E}^+_{m+1} = \frac{2\nu}{x}\widetilde{E}^+_m - \widetilde{E}^+_{m-1} \tag{S50}$$

where we have defined $\nu \equiv x - (m - m_2)$ and $x \equiv 2/\alpha_2$. In terms of the variables ν and x, the solution to this recurrence is a linear combination of the Bessel functions $E^+_m = aJ_\nu(x) + bY_\nu(x)$, just as in the $m = m_1$ case. In particular, the mapping from the $m = m_1$ case is exact under the switch $m \leftrightarrow m_1$ (so as to obtain the modified m-dependence of ν) and subsequent replacements $m_1, \alpha_1 \to m_2, \alpha_2$. Applying this transformation to the linear combination of asymptotic Bessel functions (S45) gives

$$E^+_m = \begin{cases} \dfrac{1}{\sqrt[4]{4 - a_m^2}} \left[\sqrt{\dfrac{\alpha_2}{2\pi}} \left(a e^{i\pi/4} - b e^{-i\pi/4} \right) \exp\left\{ i \int_{m_2}^{m} \cos^{-1}\left(\frac{a_k}{2}\right) \mathrm{d}k \right\} + \text{C.C.} \right] & (m_2 < m) \\ \dfrac{1}{\sqrt[4]{a_m^2 - 4}} \left[-b\sqrt{\dfrac{2\alpha_2}{\pi}} \exp\left\{ \int_m^{m_2} \cosh^{-1}\left(\frac{a_k}{2}\right) \mathrm{d}k \right\} + a\sqrt{\dfrac{\alpha_2}{2\pi}} \exp\left\{ -\int_m^{m_2} \cosh^{-1}\left(\frac{a_k}{2}\right) \mathrm{d}k \right\} \right] & (m_2 > m) \end{cases} \tag{S51}$$

as the asymptotic solution for the field E^+_m near the turning point m_2. Comparing this result with the relevant regions of our discrete WKB solution (S48) and eliminating the intermediate coefficients a and b yields

$$\begin{aligned} F &= e^{-i\pi/4}\left(Ce^{\gamma} + \frac{iD}{2} e^{-\gamma} \right) \\ G &= e^{+i\pi/4}\left(Ce^{\gamma} - \frac{iD}{2} e^{-\gamma} \right) \end{aligned} \tag{S52}$$

These are the matching relations across the $m = m_2$ turning point.

A.3. Matching Across Entire Even Stopband

Eliminating the coefficients C and D in the matching relations (S46) and (S52) finally gives

$$\begin{aligned} A &= \left(e^{\gamma} + \frac{1}{4} e^{-\gamma} \right) F + i \left(e^{\gamma} - \frac{1}{4} e^{-\gamma} \right) G \\ B &= -i \left(e^{\gamma} - \frac{1}{4} e^{-\gamma} \right) F + \left(e^{\gamma} + \frac{1}{4} e^{-\gamma} \right) G \end{aligned} \tag{S53}$$

These are the discrete WKB connection formulae across an entire $a_m > 2$ stopband and are identical to the connection formulae across a potential barrier in the standard, continuous WKB approximation [11].

B. Odd Stopband Connection Formulae

Now consider an $a_m < -2$ stopband for $m \in [m_1, m_2]$ (where m_1, m_2 are not necessarily integers), surrounded on either side by propagation bands $|a_m| < 2$. We can transform the solution E^+_m in this odd stopband region, given again by Eq. (S36), to a solution in the region near an even stopband by taking

$$\begin{aligned} a_m &\to \widetilde{a}_m \equiv -a_m \\ E^+_m &\to \widetilde{E}^+_m \equiv (-1)^m E^+_m \end{aligned} \tag{S54}$$

which leaves the recursion relation (S12) unchanged. This transformation can be achieved by multiplying (S36) by $(-1)^m$ and using the identities $\cos^{-1}(a_m/2) = \pi - \cos^{-1}(\widetilde{a}_m/2)$ and $(-1)^m e^{\pm im\pi} = 1$. Effecting this transformation yields

$$\widetilde{E}^+_m = \begin{cases} \dfrac{1}{\sqrt[4]{4 - \widetilde{a}_m^2}} \left[\widetilde{A} \exp\left\{ i \int_m^{m_1} \cos^{-1}\left(\frac{\widetilde{a}_k}{2}\right) \mathrm{d}k \right\} + \widetilde{B} \exp\left\{ -i \int_m^{m_1} \cos^{-1}\left(\frac{\widetilde{a}_k}{2}\right) \mathrm{d}k \right\} \right] & (m < m_1) \\ \dfrac{1}{\sqrt[4]{4 - \widetilde{a}_m^2}} \left[\widetilde{F} \exp\left\{ -i \int_{m_2}^{m} \cos^{-1}\left(\frac{\widetilde{a}_k}{2}\right) \mathrm{d}k \right\} + \widetilde{G} \exp\left\{ i \int_{m_2}^{m} \cos^{-1}\left(\frac{\widetilde{a}_k}{2}\right) \mathrm{d}k \right\} \right] & (m_2 < m) \end{cases} \tag{S55}$$

where we have defined

$$\begin{aligned} \widetilde{A} &= e^{-im_1\pi} B \\ \widetilde{B} &= e^{+im_1\pi} A \\ \widetilde{F} &= e^{-im_2\pi} G \\ \widetilde{G} &= e^{+im_2\pi} F \end{aligned} \tag{S56}$$

Since the transformed variable $\widetilde{a}_m$ describes an even $\widetilde{a}_m \equiv -a_m > 2$ stopband, we can apply the even stopband connection formulae (S53) to the transformed discrete WKB solution (S55) and match the transformed coefficients $\widetilde{A}, \ldots, \widetilde{G}$. Applying this even stopband matching and subsequently transforming back to the original coefficients $A, \ldots, G$ finally gives

$$B = e^{+im_1\pi}\left[e^{-im_2\pi}\left(e^{\gamma}+\frac{1}{4}e^{-\gamma}\right)G + ie^{+im_2\pi}\left(e^{\gamma}-\frac{1}{4}e^{-\gamma}\right)F\right] \tag{S57}$$
$$A = e^{-im_1\pi}\left[-ie^{-im_2\pi}\left(e^{\gamma}-\frac{1}{4}e^{-\gamma}\right)G + e^{+im_2\pi}\left(e^{\gamma}+\frac{1}{4}e^{-\gamma}\right)F\right]$$

where

$$\gamma = \int_{m_1}^{m_2}\cosh^{-1}\left(\frac{\widetilde{a}_m}{2}\right)\mathrm{d}m = \int_{m_1}^{m_2}\cosh^{-1}\left(-\frac{a_m}{2}\right)\mathrm{d}m. \tag{S58}$$

These are the discrete WKB connection formulae across an entire odd stopband and are precisely the relations contained in Eq. (S14). Interestingly, odd stopbands have no analogy in the continuous WKB approximation, and the odd stopband connection formulae (S14) are not identical to the even stopband/continuous WKB connection formulae (S53). In particular, the presence of additional turning point phases $\exp\left(\pm im_{1,2}\pi\right)$ in the odd stopband connection formulae (S57) has important consequences in quantum mechanical applications [9].

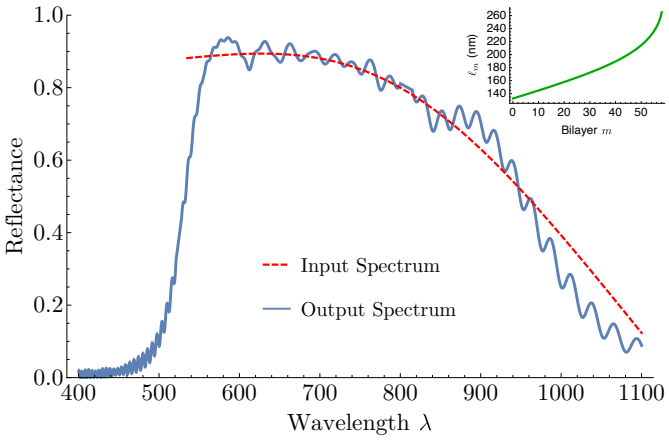

Fig. S1. A desgined reflectance spectrum with a sharp lower cut-off and slow upper roll-off. The desired spectrum (red, dashed) is put into the chirp differential equation (S59) with $n_H = 1.54$ and $n_L = 1.34$, which is then solved numerically to give the chirp function ℓ_m plotted in the inset (green). Finally, the reflectance of the computed chirp ℓ_m is found numerically via the transfer matrix method and plotted (blue). Good agreement between the input and output spectra demonstrate the accuracy of the design.

4. REVERSE-ENGINEERED SPECTRA VIA CHIRP DIFFERENTIAL EQUATION

In the main text, we show that a desired average reflectance spectrum $\widetilde{R}(\lambda)$ can be achieved via a chirped multilayer with optical thickness chirp ℓ_m satisfying the differential equation

$$\frac{\mathrm{d}\ell}{\mathrm{d}m} = \frac{-4\rho^2\sin^2\left(\frac{\pi}{1+\Xi}\right)}{\log\left[1-\widetilde{R}\Big(\lambda = 2\left(1+\Xi\right)\ell\Big)\right]}\ell. \tag{S59}$$

In this section we exhibit an additional, biologically-relevant example of reflectance spectra reverse-engineered in this way.

In Fig. S1 we exhibit a chirped multilayer with a reflectance spectrum having a sharp lower-wavelength cut-off and slow upper-wavelength roll-off. Reflectors with such properties have been found in beetle cuticles [14]. The designed reflectance spectrum in Fig. S1 shows that such optical behavior can be captured with chirped multilayer models.

5. TEM IMAGE ANALYSIS

In the main text, we compare the bilayer number N found in several ACPCs in nature to our predicted minimal number of bilayers $N_{\mathrm{exp/lin}}^{\gamma\sim 1}$ in the case of exponential and linear chirp. This comparison requires an estimate of the optical thickness ratio

$$\Xi = \left(\ell_L\right)_m / \left(\ell_H\right)_m = n_L\left(d_L\right)_m / n_H\left(d_H\right)_m, \tag{S60}$$

which we estimate for each biological ACPC via analysis of TEM images given in the relevant reference. In this section we detail the image analysis process, a sketch of which is shown in Fig. S2, using the elytra of the golden *Chrysina aurigans* beetle [15] as an example.

First, an anisotropic Gaussian filter is applied to the TEM image along the assumed axis of the ACPC, which smooths the image while highlighting the low- and high-index layers. Then a curvature flow filter is applied in order further smooth the image while preserving the edges between low- and high-index layers. Finally we binarize the image, where the binarization thresholds are determined locally in the image in order isolate the the low- and high-index layers.

After binarization, we take a thin (few pixel high) horizontal cross-section of the image, from which the layer thicknesses $\left(d_{L/H}\right)_m$ and hence local optical thickness ratios Ξ_m (S60) can be determined. The value of Ξ_m for each bilayer m in the *C. aurigans* TEM image is plotted in Fig. S3. The fixed ratio Ξ is finally estimated by taking the average optical thickness ratio $\Xi = \mu_\Xi$ over all the ACPC bilayers m.

REFERENCES

1. A. Garg, "Application of the discrete Wentzel-Kramers-Brillouin method to spin tunneling," Journal of Mathematical Physics **39**, 5166–5179 (1998).
2. S. J. Orfanidis, *Electromagnetic Waves and Antennas* (Rutgers University New Brunswick, NJ, 2002).
3. H. Bremmer, "The propagation of electromagnetic waves through a stratified medium and its WKB approximation for oblique incidence," Physica **15**, 593 – 608 (1949).

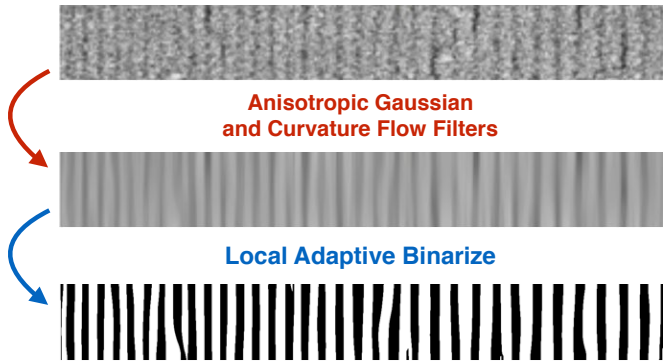

Fig. S2. Sketch of our TEM image analysis procedure applied to the ACPC in the elytra of the golden *C. aurigans* beetle. Original TEM image (top) taken from Ref. [15].

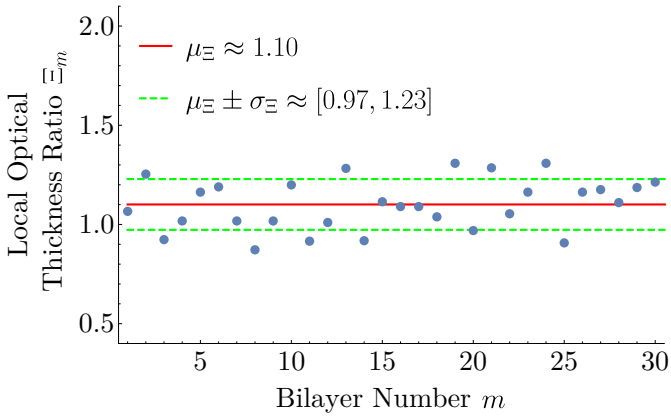

Fig. S3. Plot of the local optical thickness ratios Ξ_m calculated for each bilayer m in the *C. aurigans* TEM image shown in Fig. S2. The Ξ_m values for the first and last measured bilayers are discared to account for possible incomplete cropping of the original TEM image. The mean optical thickness ratio μ_Ξ and the standard deviations $\mu_\Xi \pm \sigma_\Xi$ about the mean are also shown.

4. M. V. Berry and K. E. Mount, "Semiclassical approximations in wave mechanics," Reports on Progress in Physics **35**, 315 (1972).
5. R. B. Dingle and G. J. Morgan, "WKB methods for difference equations I," Applied Scientific Research **18**, 221–237 (1968).
6. P. A. Braun, "WKB method for three-term recursion relations and quasienergies of an anharmonic oscillator," Theoretical and Mathematical Physics **37**, 1070–1081 (1978).
7. P. Wilmott, "A note on the WKB method for difference equations," IMA Journal of Applied Mathematics **34**, 295–302 (1985).
8. J. S. Geronimo and D. T. Smith, "WKB (Liouville-Green) analysis of second order difference equations and applications," Journal of Approximation Theory **69**, 269 – 301 (1992).
9. P. A. Braun, "Discrete semiclassical methods in the theory of Rydberg atoms in external fields," Rev. Mod. Phys. **65**, 115–161 (1993).
10. A. Garg, "Oscillatory tunnel splittings in spin systems: A discrete Wentzel-Kramers-Brillouin approach," Phys. Rev. Lett. **83**, 4385–4388 (1999).
11. E. Merzbacher, *Quantum Mechanics* (Wiley, New York, 1998), 3rd ed.
12. N. W. Ashcroft and N. D. Mermin, *Solid State Physics* (Saunders College, 1976).
13. M. Abramowitz and I. A. Stegun, *Handbook of Mathematical Functions with Formulas, Graphs, and Mathematical Tables* (Dover, 1964). Tenth printing, with corrections (December 1972).
14. W. E. Vargas, M. Hernández-Jiménez, E. Libby, D. E. Azofeifa, Á. Solis, and C. Barboza-Aguilar, "Broadening of effective photonic band gaps in biological chiral structures: From intrinsic narrow band gaps to broad band reflection spectra," EPL (Europhysics Letters) **111**, 64001 (2015).
15. E. Libby, D. E. Azofeifa, M. Hernández-Jiménez, C. Barboza-Aguilar, A. Solís, I. García-Aguilar, L. Arce-Marenco, A. Hernández, and W. E. Vargas, "Light reflection by the cuticle of C. aurigans scarabs: a biological broadband reflector of left handed circularly polarized light," Journal of Optics **16**, 082001 (2014).